Supramolecular Chemistry

How to cite: *Angew. Chem. Int. Ed.* **2021**, *60*, 10858–10864
International Edition: doi.org/10.1002/anie.202100729
German Edition: doi.org/10.1002/ange.202100729

Making Waxy Salts in Water: Synthetic Control of Hydrophobicity for Anion-Induced and Aggregation-Enhanced Light Emission

*Soohyung Kim, Jongmin Kim, and Dongwhan Lee**

Abstract: *We show that multipodal polycationic receptors function as anion-responsive light-emitters in water. Prevailing paradigms utilize rigid holes and cavities for ion recognition. We instead built open amphiphilic scaffolds that trigger polar-to-nonpolar environment transitions around cationic fluorophores upon anion complexation. This ion-pairing and aggregation event produces a dramatic enhancement in the emission intensity, as demonstrated by perchlorate as a non-spherical hydrophobic anion model. A synergetic interplay of C−H⋯anion hydrogen bonding and tight anion–π^+ contacts underpins this supramolecular phenomenon. By changing the aliphatic chain length, we demonstrate that the response profile and threshold of this signaling event can be controlled at the molecular level. With appropriate molecular design, inherently weak, ill-defined, and non-directional van der Waals interaction enables selective, sensitive, and tunable recognition in water.*

Introduction

Molecular recognition in water is an unperfected art in synthetic supramolecular chemistry.[1] As a molecule, H_2O is an unrelenting and robust competitor for hydrogen bonding (HB). As a medium, it is a strong dielectric that effectively screens electrostatic attractions.[2] While directional non-covalent bonds such as HB or dipole–dipole interactions have been widely exploited in supramolecular design, their strength becomes significantly attenuated in water.[3] In contrast, the hydrophobic effect is maximized in water, but this non-directional, weak, and ill-defined interaction is difficult to control and quantify.[4]

In this paper, we disclose the chemistry of multicationic fluorophores and their applications for anion detection in water. Taking non-conjugated 1,3,5-substituted benzene as a core structural platform, three fluorogenic pendants and three hydrophobic tails are installed in an alternating fashion (Figure 1). A synergistic interplay of C−H⋯anion HB and intimate anion–π^+ interactions results in a dramatic enhancement in fluorescence intensity through hydrophobic collapse and salt aggregation. By systematically varying the alkyl chain length, we further demonstrate that the inherent hydrophobicity of these fluorogenic cations can be controlled at the molecular level to modulate their sensitivity toward ClO_4^- in water.

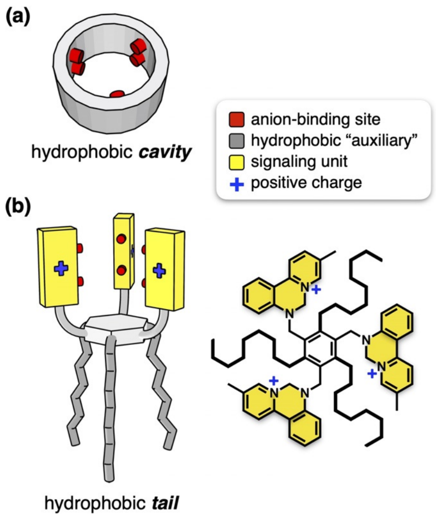

Figure 1. Schematic representations of two different strategies to control hydrophobicity for molecular recognition. a) Binding sites are located inside a hydrophobic surface. b) Binding sites are exposed to the open space, yet conformationally preorganized and spatially decoupled from aliphatic chains that facilitate ion recognition and aggregation process in water.

Background and Design Principles

Supramolecular Chemistry of Ions

Recognition of ionic species in an aqueous environment is a topic of significant importance in environmental and biological sciences.[5] Cations engage in ion–dipole interactions with macrocyclic or cage-like receptors. The concept of “hole size fitting” has been successfully implemented here by matching the host cavity size to the radius of the cations to be detected or sequestered.[6] For anions, the situation becomes more challenging. Compared with isoelectronic cations, anions are larger in size.[7] A lower ratio of charge-to-radius makes electrostatic attraction less effective.

Selective detection of large, non-spherical, and charge-diffuse anions is even more challenging if one relies solely on electrostatic interactions.[8] There is no general rule to construct host molecules by simply matching the size or the geometry of irregularly-shaped and hydrophobic anions. Moreover, a majority of known anion receptors work mostly in organic-aqueous mixed-solvent systems. Due to the intrin-

---

[*] S. Kim, J. Kim, Prof. Dr. D. Lee
Department of Chemistry, Seoul National University
1 Gwanak-ro, Gwanak-gu, Seoul 08826 (Korea)
E-mail: dongwhan@snu.ac.kr

Supporting information and the ORCID identification number(s) for the author(s) of this article can be found under: https://doi.org/10.1002/anie.202100729.

sic hydrophobicity of π-conjugated molecules, anion-responsive fluorophores operating in water are rarer still.[1,5]

Design Principles

Nature utilizes weak non-covalent interactions to recognize guests in water with remarkable selectivity and efficiency.[9] For example, the strength of electrostatic and hydrogen-bonding interactions is augmented by hydrophobic cavities or channels that effectively protect binding sites from competing water molecules. Artificial receptors[10] have been designed and synthesized to mimic binding in the "dehydrated" interior space (Figure 1 a). Such strategy is effective for the recognition of small guests, yet it is challenging to customize the shape and size of the cavity while maintaining specific binding sites at designated positions on the inner wall.[4a] While the space enclosed by the molecular skeleton is geometrically well-defined, it also becomes the upper limit in the size scale of the guest species to be entrapped.

Instead of using the rigid hydrophobic "cavity" (Figure 1 a), we decided to use flexible aliphatic "tails" (Figure 1 b and Scheme 1) to build a low-dielectric environment that promotes ion-pairing between cationic host and anionic guest in water. Among many branched molecular scaffolds in supramolecular chemistry,[11] the privileged 1,3,5-trisubstituted benzene[12] is ideally suited for our purpose, since it allows spatial decoupling of (i) cationic and fluorogenic recognition/reporter module (Scheme 1 a), and (ii) hydrophobicity controller module (Scheme 1 b). Through "steric gearing", these two functional components are placed alternately above and below the benzene plane, and do not interfere with each other when integrated into a single molecular platform (Figure 1 b), thus allowing for systematic investigation of structure–property relationships.

In addition to functioning as a conformational lock, the 2,4,6-trialkyl substituents in our system (Scheme 1 b) actively participate in the recognition of hydrophobic anion by assisting and regulating salt aggregation and fluorescence enhancement. In the following sections are described important lessons that we learned from these new amphiphilic fluorophores.

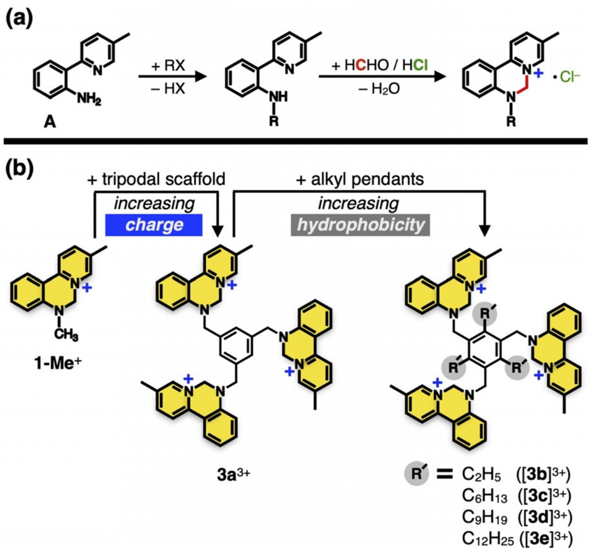

Scheme 1. Modular construction and structural elaboration.

Results and Discussion

Design and Synthesis of Model Fluorophore

As a first step to realize the idea outlined in Figure 1 b, we designed the simplest molecular prototype [**1-Me**]Cl (Scheme 1 b). This compound was prepared by following the general synthetic protocol outlined in Scheme 1 a, starting with methylation of the anilido-pyridine precursor **A**,[13] followed by acid-catalyzed condensation reaction with formaldehyde in HCl/1,4-dioxane (Scheme S1).[14] The resulting yellow precipitate was isolated by simple filtration.

A single-crystal X-ray crystallographic (SC-XRD) study on [**1-Me**]Cl confirmed the chemical connectivity, with the C–H groups of the pyridinium ring and the methylene bridge pointing to the same direction (Figure 2 a). The molecular electrostatic potential (MEP) map predicted that the two carbon atoms (C1 and C2) associated with these C–H bonds are the most electron-deficient sites (Figure 2 b). The highly polarized nature of these C–H groups suggested their potential role as hydrogen-bonding donor (HBD) toward anionic species X^- as hydrogen-bonding acceptor (HBA).[15] This idea prompted our investigation of multicationic molecules derived from [**1-Me**]$^+$ that can engage in multiple C–H···X^- contacts to make stronger adducts (vide infra).

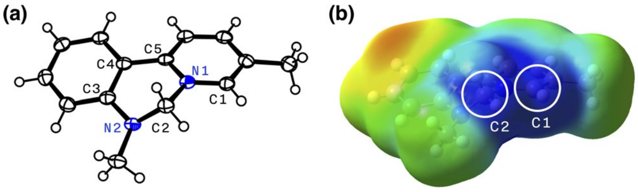

Figure 2. a) X-ray structure of [**1-Me**]$^+$ cation as ORTEP diagrams with thermal ellipsoids at the 50% probability level. Torsional angle for N1-C5-C4-C3 = 15.3°. b) Molecular electrostatic potential (MEP) map of [**1-Me**]$^+$ cation calculated by B3LYP-D3/6-31G(d,p) level of theory. The circled regions (white) denote the C1 and C2 atoms.[20]

Multicationic Molecular Scaffolds

By substitution reactions of the common intermediate **A**, a series of cationic molecules were prepared in a straightforward manner. As summarized in Scheme 2, the chloride salt of tricationic [**3a**]$^{3+}$ was synthesized via substitution reactions between **A** and 1,3,5-tribromomethyl benzene, followed by acid-catalyzed condensation reactions with formaldehyde. Both reactions proceeded in good yields (> 85 %). For comparative studies, dicationic [**2**]$^{2+}$ and monocationic [**1-Bz**]$^+$ were also prepared through the same procedure by using 1,3-dibromomethyl benzene and bromomethyl benzene, respectively (Scheme 2).

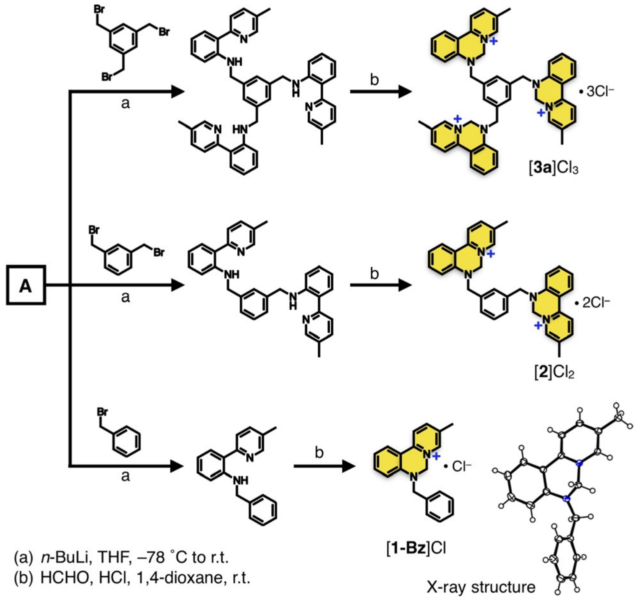

Scheme 2. Synthesis of mono-, di-, and tricationic fluorophores.[20]

In the solid-state, [**3a**]Cl_3 is fluorescent ($\lambda_{max,em} = 585$ nm; $\Phi_F = 4.9\,\%$), but the emission is essentially quenched in H_2O ($\lambda_{max,em} = 590$ nm; $\Phi_F < 1.0\,\%$) (Figure S1). A similar behavior was observed for the fluorophore core model [**1-Me**]Cl with $\lambda_{max,em} = 555$ nm ($\Phi_F = 27.8\,\%$) in the solid-state, and $\lambda_{max,em} = 610$ nm ($\Phi_F < 1.0\,\%$) in H_2O. In terms of the electronic excitation, [**3a**]Cl_3 in H_2O ($\lambda_{max,abs} = 400$ nm; $\varepsilon = 10\,205$ cm^{-1}M^{-1}) behaves like a simple sum of electronically independent chromophores that retain the photophysical properties of the [**1-Me**]Cl ($\lambda_{max,abs} = 400$ nm; $\varepsilon = 3648$ cm^{-1}M^{-1} in H_2O) as local site model (Figure S2). In support of this notion, [**3a**]Cl_3, [**2**]Cl_2, and [**1-Bz**]Cl also share similar absorption and emission features arising from localized light-absorbing and emitting units with no significant electronic coupling (Figure S3).

Aggregation-Induced Fluorescence Enhancement

The phase-dependent fluorescence properties of [**3a**]Cl_3 (Figure S1) prompted us to investigate the effects of fluid-to-solid environment change on the excited-state photophysics. Since [**3a**]Cl_3 is highly soluble in water, we decided to add less polar organic solvent THF to induce aggregation in H_2O–THF mixed-solvent system (Figure 3). No significant change was observed in fluorescence upon addition of THF with a volume fraction (f_{THF}) of below 90%. However, when the f_{THF} value exceeded 95%, the emission intensity was gradually increased, resulting in 5-fold enhancement at $f_{THF} = 99\,\%$, with a slight blue shift ($\lambda_{max,em} = 580$ nm). Such optical response has its origin in the aggregation-induced emission, which was confirmed by dynamic light scattering (DLS) studies conducted under the same conditions (Figure S4).

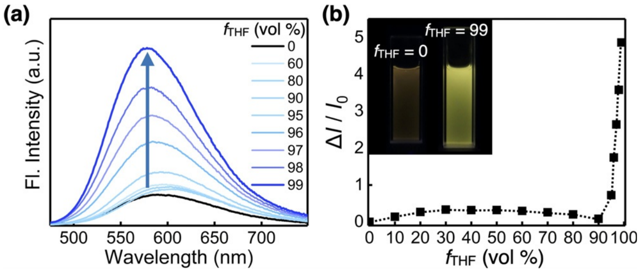

Figure 3. a) Changes in the fluorescence spectra ($\lambda_{exc} = 400$ nm) of [**3a**]Cl_3 (0.100 mM) with increasing volume fraction of THF (f_{THF}) in H_2O–THF mixed solvent system at $T = 293$ K. b) Plot of emission intensity enhancement factor ($\Delta I/I_0$) at $\lambda = 580$ nm vs. f_{THF}. Inset: photographs of [**3a**]Cl_3 at $f_{THF} = 0\,\%$ (left) and 99% (right) under UV lamp irradiation ($\lambda = 365$ nm).

Specific Interactions Between the Fluorophore and Hydrophobic Anion

Intrigued by the fluorescence turn-on response of [**3a**]Cl_3 in the hydrophobic environment (Figure 3), we proceeded to test the feasibility of inducing self-assembly in water by using hydrophobic anions instead. A preliminary screening showed that an aqueous solution of [**3a**]Cl_3 (3.3 mM) immediately produces precipitates upon treatment with $NaClO_4$ (50 equiv). This anion metathesis reaction product [**3a**]$(ClO_4)_3$ was subsequently characterized by SC-XRD (Figure 4).

As shown in Figures 4 and S5a, the solid-state structure of [**3a**]$(ClO_4)_3$ revealed the presence of both C–H⋯anion hydrogen bonds and intimate anion–π^+ contacts between the fluorophore and perchlorate anion. We found that the highly polarized pyridinium C–H bond and the methylene bridge C–H groups engage in dipole–anion interactions with $d_{C-H\cdots O} = 3.303(4)$–$3.504(3)$ Å and $d_{C-H\cdots O} = 3.291(3)$–3.449-

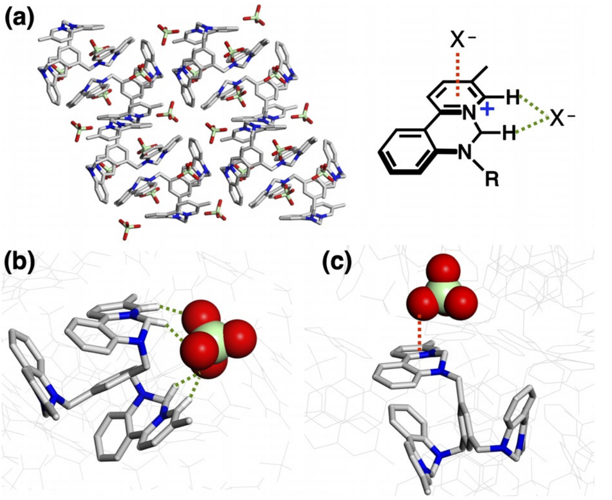

Figure 4. a) Capped-stick representation of the crystal packing structure of [**3a**]$(ClO_4)_3$ based on crystallographically determined atomic coordinates. Hydrogen atoms are omitted for clarity. Close-up views of b) C–H⋯ClO_4^- hydrogen bonding (green dashed lines), and c) anion–π^+ contacts (red dashed lines).[20]

(3) Å, respectively. In addition, the oxygen atom of ClO_4^- is pointing to the centroid of pyridinium moiety of **[3a]**$^{3+}$ with $d_{\text{pyridinium}\cdots O} = 3.083(2)$ Å, which is within the range of typical anion–π interactions.[16] The X-ray structures of [**1-Bz**](ClO_4) and [**2**]$(ClO_4)_2$ (Figures S5b, S5c, S6, and S7) consistently show similar C–H···anion and anion–π^+ contacts as well, thus confirming that these non-covalent interactions are position specific, not biased by crystal packing.

In stark contrast to the perchlorate salts (Figures 4, S6, and S7), the X-ray structures of the corresponding chloride salts [**1-Me**]Cl and [**1-Bz**]Cl do not show any anion–π^+ interactions (Figures S8 and S9). Only C–H···Cl^- hydrogen bonds were observed for the polarized (see the MEP map in Figure 2b) pyridinium C–H bonds ($d_{C\text{–}H\cdots Cl} = 3.3948(18)$–$3.6635(17)$ Å) and methylene C–H groups ($d_{C\text{–}H\cdots Cl} = 3.4892(19)$–$3.5035(18)$ Å). This contrasting behavior implicates that the cationic fluorophore can engage in different types of non-covalent interactions depending on the nature of the anion. For large and charge-diffuse (= "soft") ClO_4^-, both C–H···anion and anion–π^+ interactions are involved, whereas C–H hydrogen bonding is mainly utilized for small and compact (= "hard") Cl^-.

To confirm that the non-covalent interactions observed in the solid-state are not crystal packing artifacts, we proceeded to carry out ^{1}H NMR spectroscopic studies in solution. To mimic the relatively non-polar environment of the solid-state, CD_2Cl_2 was chosen as a solvent. As shown in Figure 5, the ^{1}H NMR spectra of [**3a**]Cl_3 and [**3a**]$(ClO_4)_3$ show significant differences in the pyridinium C–H ($\Delta\delta = 1.26$ ppm, green square) and methylene CH_2 ($\Delta\delta = 0.60$ ppm, green circle) proton resonances, while the rest of the signals in the aromatic region are shifted only to a small extent.

This behavior supports the notion that the crystallographically observed C–H···anion interactions (Figure 4) are maintained in the solution phase as well. The larger electrostatic contribution of harder anion to the hydrogen bonding is reflected on the large and systematic downfield shifts of the participating protons when comparison is made between C–H···Cl^- and C–H···ClO_4^-. Comparative studies on [**1-Bz**]Cl vs. [**1-Bz**](ClO_4) (Figure 5), and [**2**]Cl_2 vs. [**2**]$(ClO_4)_2$ (Figure S10) further validate this interpretation, and support the general applicability of our anion recognition model.

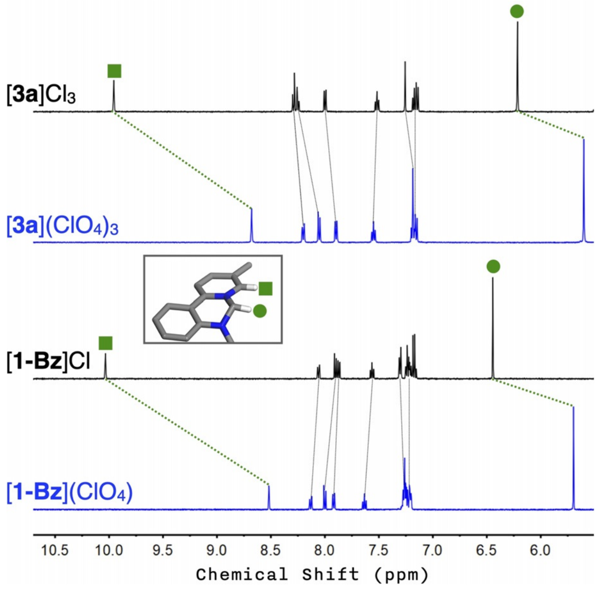

Figure 5. Partial ^{1}H NMR spectra of [**3a**]Cl_3, [**3a**]$(ClO_4)_3$, [**1-Bz**]Cl, and [**1-Bz**](ClO_4) in CD_2Cl_2 (concentration = 1.0 mM; $T = 298$ K) with the pyridinium (square) and methylene C–H (circle) resonances denoted with symbols.

Selective Recognition of Perchlorate Anion in Water

With spectroscopic and structural evidence obtained for the specific interactions with ClO_4^- ion, we investigated the optical response of the fluorophore by titration methods. Upon addition of $NaClO_4$ (0–200 equiv), the fluorescence intensity ($\lambda_{\text{max,em}} = 570$ nm) of [**3a**]Cl_3 in water (0.100 mM) was enhanced up to 10-fold (Figure 6a). Similar fluorescence turn-on response occurred regardless of the choice of the counter cation ($LiClO_4$, $NaClO_4$, and $KClO_4$) (Figure S11), or solution pH (Figure S12b). In contrast, no spectral change was observed with hydrophilic anions, such as F^-, Cl^-, Br^-, I^-, HCO_3^-, CO_3^{2-}, AcO^-, $H_2PO_4^-$, HPO_4^{2-}, HSO_4^-, NO_3^-, ClO_3^-, and BF_4^- (all delivered as sodium salts) under identical conditions (Figure 6b). When ClO_4^- was added subsequently to the mixtures of [**3a**]Cl_3 and these hydrophilic anions, enhancement in fluorescence was consistently observed with little interference (Figure S12a).

A combination of dynamic light scattering (DLS) and SEM studies revealed that the fluorescence turn-on response is accompanied by the formation of aggregates in solution (Figure 7). An increasing amount of $NaClO_4$ produced aggregates of increasing hydrodynamic diameters (average values: 124–183 nm; Figure 7). Spherical nanoparticles of comparable sizes were also observed by SEM analysis (Figure 7, insets). For either pristine [**3a**]Cl_3 or upon treatment with lower (10 equiv) amount of $NaClO_4$, no aggregation was observed.

To investigate the effects of the overall charge of the fluorophore on the anion-induced spectral changes, compa-

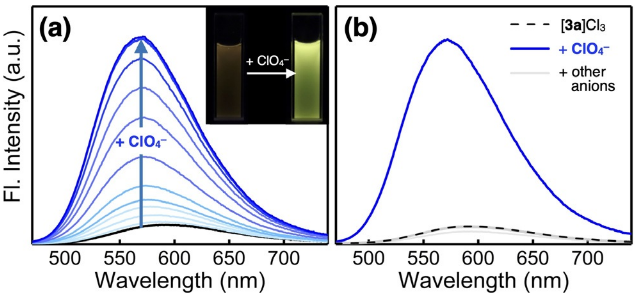

Figure 6. Changes in the fluorescence emission spectra of [**3a**]Cl_3 (0.100 mM) in H_2O (a) upon addition of $NaClO_4$ (0–200 equiv), and (b) other anions (200 equiv) including F^-, Cl^-, Br^-, I^-, HCO_3^-, CO_3^{2-}, AcO^-, $H_2PO_4^-$, HPO_4^{2-}, HSO_4^-, NO_3^-, ClO_3^-, and BF_4^- (gray lines). In (b), the emission spectra of [**3a**]Cl_3 (black dashed lines) and response to ClO_4^- (blue line) are also overlaid for comparison. $\lambda_{\text{exc}} = 400$ nm; $T = 293$ K.

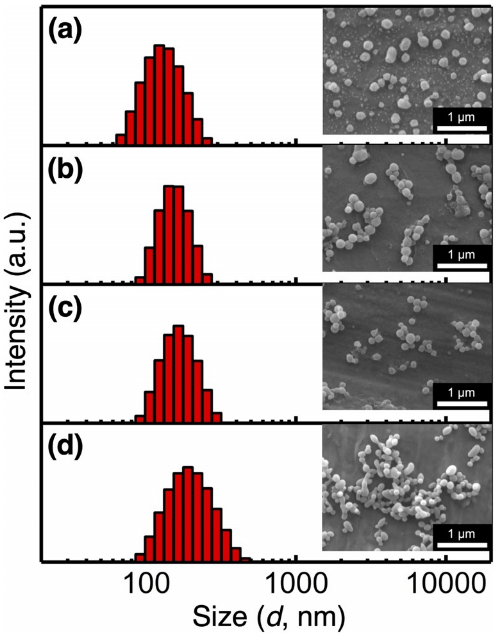

Figure 7. DLS profiles of [**3a**]Cl$_3$ (0.100 mM) in water obtained upon addition of NaClO$_4$: a) 50 equiv, b) 100 equiv, c) 150 equiv, and d) 200 equiv. Insets show the corresponding SEM images.

rative studies were carried out with monocationic [**1-Bz**]$^+$ (0.300 mM), dicationic [**2**]$^{2+}$ (0.150 mM), and tricationic [**3a**]$^{3+}$ (0.100 mM). Despite sharing the structurally identical cationic pendants attached to the benzene core, [**1-Bz**]Cl and [**2**]Cl$_2$ showed only negligible turn-on response under similar conditions (Figure S13). A higher charge density of the receptor molecule is thus important for anion binding and aggregation.

Sensitivity Control by Intrinsic Hydrophobicity

Sensitivity is as important as selectivity in chemical sensing. In the ion pairing-induced aggregation scheme, the inherent hydrophobicity of the fluorophore should impact the sensitivity towards the target anion in water. The tripodal skeleton of the first-generation molecule [**3a**]$^{3+}$ is ideally suited for this purpose since the remaining sites on the benzene core can be modified by installing alkyl groups of varying chain length (Figure 1b). The three-fold molecular symmetry effectively multiplies the substituents' hydrophobicity effects, which are essentially decoupled from the charge effects of the fluorophores appended as different branching units. Such spatial separation and functional independence are advantageous for systematic optimization of individual components.

To realize this idea, compounds [**3b**]Cl$_3$, [**3c**]Cl$_3$, [**3d**]Cl$_3$, and [**3e**]Cl$_3$ were prepared by taking the synthetic route outlined in Scheme 3. The peripheral alkyl chains are varied from ethyl to dodecyl groups to systematically increase the hydrophobicity while keeping the same cationic pendants. With increasing alkyl chain length, the fluorescence emission of these chloride salts remains essentially unchanged in water, except for only slight spectral blue shifts ($\Delta\lambda = 20$ nm) and increase in the fluorescence quantum yields of emission ($\Phi_F = 0.1$–$3.3\,\%$) (Table S2). No noticeable change was observed in the fluorescence intensity upon prolonged (up to 12 h) exposure to the excitation light source (Figure S14).

Upon addition of NaClO$_4$, all compounds displayed fluorescence turn-on response (Figures 8a and S15), albeit with varying degrees of enhancement factors and the dose-dependent growth of the saturation curves. This photophysical change is also accompanied by the formation of solution aggregates, as confirmed by DLS and SEM studies (Figure S16). With increasing alkyl chain length, the hydrodynamic diameter of the aggregates gradually decreased (160–20 nm) from [**3a**]$^{3+}$ to [**3d**]$^{3+}$, but increased to 95 nm for

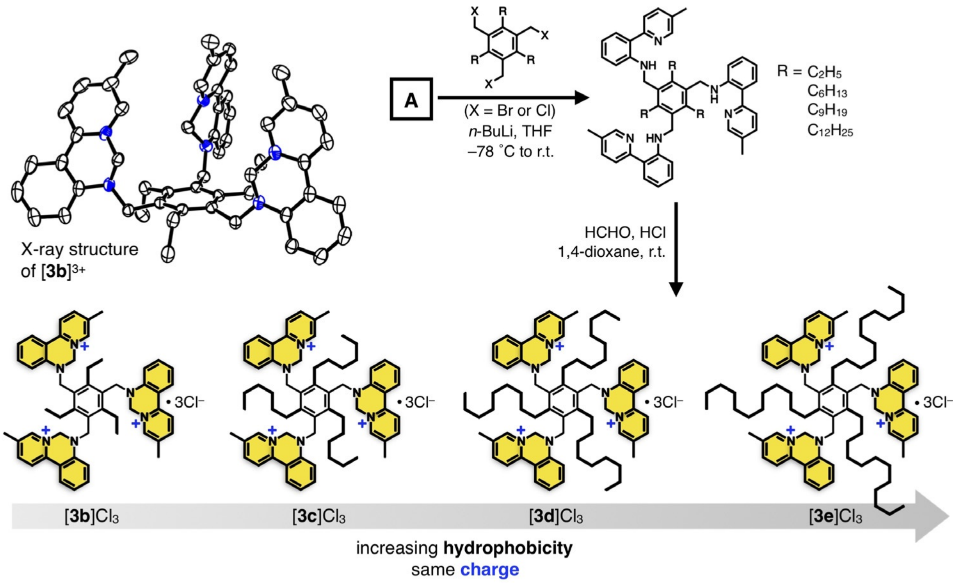

Scheme 3. Synthesis of structural variants with systematic increase in the aliphatic chain length.[20]

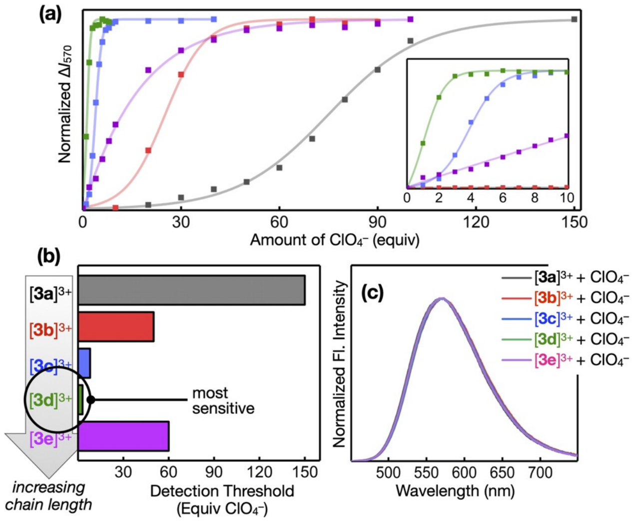

Figure 8. a) Plots of fluorescence intensity at $\lambda = 570$ nm (normalized to the maximum value, ΔI_{570} of each samples) vs. equiv of $NaClO_4$ added to [**3a**]Cl_3, [**3b**]Cl_3, [**3c**]Cl_3, [**3d**]Cl_3, and [**3e**]Cl_3 solution samples in water (concentrations = 0.100 mM). Solid lines serve as visual guides. b) Detection thresholds quantified as 95% of the final saturation value of the fluorescence turn-on response. c) Normalized fluorescence spectra ($\lambda_{exc} = 400$ nm) of the aggregates at $T = 293$ K.

[**3e**]$^{3+}$. Despite variations in size, the emission from the aggregates all converge to $\lambda_{max,em} = 570$ nm, and become indistinguishable when normalized (Figure 8c).

As a quantitative measure of sensitivity, we compared the equiv of ClO_4^- that is needed to reach 95% of the final saturation value of the fluorescence turn-on response. As shown in Figure 8b, sensitivity is improved as the alkyl chain length increases. Compared to the benchmark system [**3a**]$^{3+}$ having simple hydrogen atoms at the benzene core, [**3d**]$^{3+}$ having long nonyl chains shows ca. 50-fold enhancement in sensitivity to perchlorate anion. A complete turn-on response was achieved by adding only 3 equiv of ClO_4^- to [**3d**]$^{3+}$, which corresponds to 1 equiv of ClO_4^- relative to each fluorogenic pendant in [**3d**]$^{3+}$.[17] As in the case of [**3a**]$^{3+}$ (Figure 6b), little spectral change was observed for [**3d**]$^{3+}$ with hydrophilic anions, which do not interfere with the fluorescence turn-on response to ClO_4^- (Figure S18).

This chain-length dependent sensitivity is consistent with our expectation that longer and more hydrophobic alkyl chains would promote anion-induced aggregation in water. Deviating from this intuitive model, however, [**3e**]$^{3+}$ having the longest hydrophobic chain in our series, shows significantly diminished sensitivity. We suspect that installation of excessively long alkyl chains to enhance the hydrophobicity also increased the size mismatch of the cation-anion pair, thereby lowering the lattice energy, and making the aggregates less stable. A structural overengineering by further elongation of alkyl chain beyond [**3d**]$^{3+}$ apparently compromised both the sensitivity and the net intensity of the fluorescence signal. By chain length control, aggregation-induced emission (AIE)[18] can be regulated at the molecular level to fine-tune the sensory response in water, which is demonstrated for the first time here.

Conclusion

In water, nonpolar molecules minimize solvent-exposed surfaces by structural collapse (i.e., folding) or self-association. Oppositely-charged hydrophobic ions are also attracted to each other to form neutral salts, the decreased overall polarity of which lowers the solubility in water and induces spontaneous aggregation. We demonstrate that this convoluted process is assisted by long alkyl pendants that are strategically placed around a multipodal polycationic platform. Upon anion complexation, a polar-to-nonpolar environment change around the cationic fluorophore produces a dramatic enhancement in the fluorescence intensity by AIE.

The response profile and threshold of this signaling event can be controlled at the molecular level by changing the chain length of the amphiphilic fluorophore in water. This strategy has no previous example, and exploits inherently weak and non-directional dispersive interactions for selective, sensitive, and tunable recognition. We demonstrated its practical utility by using ClO_4^- as a model of non-spherical hydrophobic anion that is difficult to detect with conventional macrocyclic or cage-type receptors.[19] Efforts are currently underway in our laboratory to expand the scope of this chemistry by structurally more elaborate amphiphilic receptor–fluorophore conjugates.

Acknowledgements

This work was supported by the Samsung Science and Technology Foundation (SSTF-BA1701-09).

Conflict of interest

The authors declare no conflict of interest.

Keywords: aggregation · anions · fluorescence · hydrophobic effect · molecular recognition

[1] a) J. W. Steed, J. L. Atwood, *Supramolecular Chemistry*, 2nd ed., Wiley, Chichester, **2009**; b) P. S. Cremer, A. H. Flood, B. C. Gibb, D. L. Mobley, *Nat. Chem.* **2018**, *10*, 8–16; c) E. Persch, O. Dumele, F. Diederich, *Angew. Chem. Int. Ed.* **2015**, *54*, 3290–3327; *Angew. Chem.* **2015**, *127*, 3341–3382; d) G. V. Oshovsky, D. N. Reinhoudt, W. Verboom, *Angew. Chem. Int. Ed.* **2007**, *46*, 2366–2393; *Angew. Chem.* **2007**, *119*, 2418–2445; e) S. M. Biros, J. Rebek, Jr., *Chem. Soc. Rev.* **2007**, *36*, 93–104.

[2] a) G. Hummer, *Nat. Chem.* **2010**, *2*, 906–907; b) D. Laage, J. T. Hynes, *Science* **2006**, *311*, 832–835.

[3] a) M. J. Langton, C. J. Serpell, P. D. Beer, *Angew. Chem. Int. Ed.* **2016**, *55*, 1974–1987; *Angew. Chem.* **2016**, *128*, 2012–2026; b) A. P. Davis, S. Kubik, A. Dalla Cort, *Org. Biomol. Chem.* **2015**, *13*, 2499–2500; c) E. Klein, Y. Ferrand, N. P. Barwell, A. P. Davis, *Angew. Chem. Int. Ed.* **2008**, *47*, 2693–2696; *Angew. Chem.* **2008**, *120*, 2733–2736.

[4] a) H. Yao, H. Ke, X. Zhang, S.-J. Pan, M.-S. Li, L.-P. Yang, G. Schreckenbach, W. Jiang, *J. Am. Chem. Soc.* **2018**, *140*, 13466–13477; b) D. Ben-Amotz, *Annu. Rev. Phys. Chem.* **2016**, *67*, 617–638; c) P. W. Snyder, J. Mecinović, D. T. Moustakas, S. W. Thomas, M. Harder, E. T. Mack, M. R. Lockett, A. Héroux, W.

Sherman, G. M. Whitesides, *Proc. Natl. Acad. Sci. USA* **2011**, *108*, 17889–17894.

[5] a) N. Busschaert, C. Caltagirone, W. Van Rossom, P. A. Gale, *Chem. Rev.* **2015**, *115*, 8038–8155; b) N. H. Evans, P. D. Beer, *Angew. Chem. Int. Ed.* **2014**, *53*, 11716–11754; *Angew. Chem.* **2014**, *126*, 11908–11948; c) L. M. Salonen, M. Ellermann, F. Diederich, *Angew. Chem. Int. Ed.* **2011**, *50*, 4808–4842; *Angew. Chem.* **2011**, *123*, 4908–4944.

[6] a) S.-i. Kang, M. Lee, D. Lee, *J. Am. Chem. Soc.* **2019**, *141*, 5980–5986; b) J. Murray, K. Kim, T. Ogoshi, W. Yao, B. C. Gibb, *Chem. Soc. Rev.* **2017**, *46*, 2479–2496; c) G. W. Gokel, W. M. Leevy, M. E. Weber, *Chem. Rev.* **2004**, *104*, 2723–2750.

[7] Y. Marcus, *Chem. Rev.* **1988**, *88*, 1475–1498.

[8] a) A. Borissov, I. Marques, J. Y. C. Lim, V. Félix, M. D. Smith, P. D. Beer, *J. Am. Chem. Soc.* **2019**, *141*, 4119–4129; b) P. Molina, F. Zapata, A. Caballero, *Chem. Rev.* **2017**, *117*, 9907–9972; c) P. A. Gale, E. W. Howe, X. Wu, *Chem* **2016**, *1*, 351–422; d) S. Kubik, *Chem. Soc. Rev.* **2010**, *39*, 3648–3663.

[9] a) D. Shetty, J. K. Khedkar, K. M. Park, K. Kim, *Chem. Soc. Rev.* **2015**, *44*, 8747–8761; b) P. Aryal, M. S. P. Sansom, S. J. Tucker, *J. Mol. Biol.* **2015**, *427*, 121–130; c) H. Yang, M. W. Wong, *J. Am. Chem. Soc.* **2013**, *135*, 5808–5818.

[10] a) T. Muraoka, D. Noguchi, R. S. Kasai, K. Sato, R. Sasaki, K. V. Tabata, T. Ekimoto, M. Ikeguchi, K. Kamagata, N. Hoshino, H. Noji, T. Akutagawa, K. Ichimura, K. Kinbara, *Nat. Commun.* **2020**, *11*, 2924; b) W. Liu, S. K. Samanta, B. D. Smith, L. Isaacs, *Chem. Soc. Rev.* **2017**, *46*, 2391–2403; c) K. Ariga, T. Kunitake, *Acc. Chem. Res.* **1998**, *31*, 371–378.

[11] a) N. Lau, L. N. Zakharov, M. D. Pluth, *Chem. Commun.* **2018**, *54*, 2337–2340; b) A. E. Hargrove, S. Nieto, T. Zhang, J. L. Sessler, E. V. Anslyn, *Chem. Rev.* **2011**, *111*, 6603–6782; c) P. Ballester, *Chem. Soc. Rev.* **2010**, *39*, 3810–3830; d) B. Kuswandi, Nuriman, W. Verboom, D. N. Reinhoudt, *Sensors* **2006**, *6*, 978–1017.

[12] a) S. Saha, B. Akhuli, S. Chakraborty, P. Ghosh, *J. Org. Chem.* **2013**, *78*, 8759–8765; b) S. Sambasivan, S.-G. Kim, S. M. Choi, Y. M. Rhee, K. H. Ahn, *Org. Lett.* **2010**, *12*, 4228–4231; c) A. Vacca, C. Nativi, M. Cacciarini, R. Pergoli, S. Roelens, *J. Am. Chem. Soc.* **2004**, *126*, 16456–16465; d) G. Hennrich, E. V. Anslyn, *Chem. Eur. J.* **2002**, *8*, 2218–2224.

[13] H. Park, H. M. Ahn, H. Y. Jeong, C. Kim, D. Lee, *Chem. Eur. J.* **2018**, *24*, 8632–8638.

[14] J. T. Hutt, Z. D. Aron, *Org. Lett.* **2011**, *13*, 5256–5259.

[15] a) Y. Liu, W. Zhao, C.-H. Chen, A. H. Flood, *Science* **2019**, *365*, 159–161; b) L. M. Eytel, H. A. Fargher, M. M. Haley, D. W. Johnson, *Chem. Commun.* **2019**, *55*, 5195–5206; c) A. Sengupta, Y. Liu, A. H. Flood, K. Raghavachari, *Chem. Eur. J.* **2018**, *24*, 14409–14417.

[16] a) J. Wang, X. Gu, P. Zhang, X. Huang, X. Zheng, M. Chen, H. Feng, R. T. K. Kwok, J. W. Y. Lam, B. Z. Tang, *J. Am. Chem. Soc.* **2017**, *139*, 16974–16979; b) A. J. Neel, M. J. Hilton, M. S. Sigman, F. D. Toste, *Nature* **2017**, *543*, 637–646; c) M. Giese, M. Albrecht, K. Rissanen, *Chem. Rev.* **2015**, *115*, 8867–8895.

[17] The fluorescence turn-on response was observed even with μM-level concentration of [**3d**]$\mathrm{Cl_3}$, albeit with a diminished level of sensitivity (Figure S17).

[18] a) N. Li, Y. Y. Liu, Y. Li, J. B. Zhuang, R. R. Cui, Q. Gong, N. Zhao, B. Z. Tang, *ACS Appl. Mater. Interfaces* **2018**, *10*, 24249–24257; b) M. Gao, B. Z. Tang, *ACS Sens.* **2017**, *2*, 1382–1399; c) J. Mei, N. L. C. Leung, R. T. K. Kwok, J. W. Y. Lam, B. Z. Tang, *Chem. Rev.* **2015**, *115*, 11718–11940.

[19] a) E. M. Zahran, E. M. Fatila, C.-H. Chen, A. H. Flood, L. G. Bachas, *Anal. Chem.* **2018**, *90*, 1925–1933; b) C. L. D. Gibb, B. C. Gibb, *J. Am. Chem. Soc.* **2011**, *133*, 7344–7347.

[20] Deposition Numbers 2052739 (for [**1-Me**]Cl), 2052740 (for [**1-Bz**]Cl), 2052742 (for [**3b**]$\mathrm{Cl_3}$), 2052743 (for [**3a**]$\mathrm{(ClO_4)_3}$), 2052744 (for [**1-Bz**]$\mathrm{(ClO_4)}$), and 2052745 (for [**2**]$\mathrm{(ClO_4)_2}$) contain the supplementary crystallographic data for this paper. These data are provided free of charge by the joint Cambridge Crystallographic Data Centre and Fachinformationszentrum Karlsruhe Access Structures service www.ccdc.cam.ac.uk/structures.

Manuscript received: January 16, 2021
Revised manuscript received: February 18, 2021
Accepted manuscript online: February 21, 2021
Version of record online: March 30, 2021